Aging Cell (2012) **11**, pp1084–1093 Doi: 10.1111/acel.12009

Tyr682 in the Aβ-precursor protein intracellular domain regulates synaptic connectivity, cholinergic function, and cognitive performance

Carmela Matrone,[1,2]* Siro Luvisetto,[1]* Luca R. La Rosa,[1] Robert Tamayev,[3] Annabella Pignataro,[1,4] Nadia Canu,[1,5] Li Yang,[6] Alessia P. M. Barbagallo,[3] Fabrizio Biundo,[3] Franco Lombino,[3] Hui Zheng,[6] Martine Ammassari-Teule[1,4] and Luciano D'Adamio[3]

[1]CNR – National Research Council, Cell Biology and Neurobiology Institute, Rome, 00143, Italy
[2]Department of Medical Biochemistry, University of Aarhus, 8000, Aarhus C, Denmark
[3]Department of Microbiology and Immunology, Einstein College of Medicine, Bronx, NY, 10461, USA
[4]Santa Lucia Foundation, Experimental Neurology Unit, Rome, 00143, Italy
[5]Department of Systems Medicine, University of Tor Vergata, Rome, 00133, Italy
[6]Huffington Center on Aging and Department of Molecular and Human Genetics, Baylor College of Medicine, Houston, TX, 77030, USA

Summary

Processing of Aβ-precursor protein (APP) plays an important role in Alzheimer's disease (AD) pathogenesis. The APP intracellular domain contains residues important in regulating APP function and processing, in particular the ^{682}YENPTY^{687} motif. To dissect the functions of this sequence *in vivo*, we created an *APP* knock-in allele mutating Y^{682} to Gly (*APP$^{YG/YG}$* mice). This mutation alters the processing of APP and TrkA signaling and leads to postnatal lethality and neuromuscular synapse defects when expressed on an *APP-like protein 2* KO background. This evidence prompted us to characterize further the *APP$^{YG/YG}$* mice. Here, we show that *APP$^{YG/YG}$* mice develop aging-dependent decline in cognitive and neuromuscular functions, a progressive reduction in dendritic spines, cholinergic tone, and TrkA levels in brain regions governing cognitive and motor functions. These data are consistent with our previous findings linking NGF and APP signaling and suggest a causal relationship between altered synaptic connectivity, cholinergic tone depression and TrkA signaling deficit, and cognitive and neuromuscular decline in *APP$^{YG/YG}$* mice. The profound deficits caused by the Y^{682} mutation underscore the biological importance of APP and indicate that *APP$^{YG/YG}$* are a valuable mouse model to study APP functions in physiological and pathological processes.

Correspondence
Carmela Matrone, Department of Medical Biochemistry, University of Aarhus, 8000 Aarhus C, Denmark. Tel.: +45 87167821; fax: +45 86131160; e-mail: matrone@biokemi.au.dk
or
Luciano D'Adamio, Department of Microbiology and Immunology, Einstein College of Medicine, Bronx, New York, NY 10461, USA. Tel.: +1 718 430 3244; fax: +1 718 430 8711; e-mail: luciano.dadamio@einstein.yu.edu

*These authors contributed equally to this work.

Accepted for publication *11 September 2012*

Key words: Alzheimer's disease; amyloid precursor protein; behavior; cholinergic system; dendritic spines; TrkA receptor; YENTPY domain.

Introduction

Aβ-precursor protein (APP) is extensively studied because processing of APP is linked to AD pathogenesis. AD is characterized by extracellular brain deposition of amyloid plaques and intraneuronal neurofibrillary lesions (Hardy & Selkoe, 2002). Amyloid plaques consist primarily of Aβ peptides, which are produced by a sequential β- and γ-secretase cleavage of APP (Hardy & Selkoe, 2002). Some familial forms of dementias are caused by mutations in either *APP* or genes that regulate APP processing, *BRI2/ITM2B* and *PSEN1/PSEN2* (Vidal *et al.*, 1999; Hardy & Selkoe, 2002; Fotinopoulou *et al.*, 2005; Matsuda *et al.*, 2005, 2008, 2011), underlying the relevance of APP processing to AD pathogenesis. The prevalent pathogenic model of AD posits that aggregates of Aβ trigger dementia (Hardy & Selkoe, 2002). However, new evidence suggests that alterations in APP functions/processing contribute to AD pathogenesis (Tamayev *et al.*, 2011, 2012), and that it is therefore important to understand the role of APP *in vivo*.

The intracellular region of APP is functionally important. Numerous proteins bind this region of APP, and these protein–protein interactions regulate the processing and functions of APP (Roncarati *et al.*, 2002; Matsuda *et al.*, 2003; Scheinfeld *et al.*, 2003a,b). Most interactions of APP involve the YENPTY sequence (amino acids 682–687, following the numbering of 695-amino-acid-long brain APP isoform). Phosphorylation of Y^{682} is consequential. Some proteins, such as Grb2 (Russo *et al.*, 2002; Zhou *et al.*, 2004), Shc (Russo *et al.*, 2002; Tarr *et al.*, 2002), Grb7, and Crk (Tamayev *et al.*, 2009), interact with APP only when Y^{682} is phosphorylated, whereas others, like Fe65, Fe65L1, and Fe65L2, only when this tyrosine is not phosphorylated (Zhou *et al.*, 2009), suggesting that phosphorylation–dephosphorylation on Y^{682} modulates APP functions.

To test the *in vivo* function of Y^{682}, we have created mice with Y^{682} replaced by G (*APP$^{YG/YG}$* mice that express the mutant APPYG protein). When this point mutation is introduced into an *APLP2-KO* background, *APP$^{YG/YG}$/APLP2$^{-/-}$* mutant mice exhibit neuromuscular synapse deficits and early lethality (Barbagallo *et al.*, 2011), similar to *APP/APLP2* double KO mice (Li *et al.*, 2010), suggesting an essential role of Y^{682} in development and/or aging. *APP$^{YG/YG}$* mice also show a decrease in APP processing by β-secretase, leading to a reduction in Aβ peptides, as compared to wild-type littermates (Barbagallo *et al.*, 2010), showing that Y^{682} plays a pivotal role in regulating APP processing.

Several data have linked TrkA signaling to APP processing (Matrone *et al.*, 2008, 2009). Conversely, *APP$^{YG/YG}$* mice have impaired NGF/TrkA signaling (Matrone *et al.*, 2011), showing that APP (and in particular Y^{682}) regulates TrkA function. Altogether, these data underscore a close crosstalk between these two membrane proteins.

Here, we have further characterized the $APP^{YG/YG}$ mice and analyzed whether this $Y^{682}G$ mutation causes developmental and/or aging-dependent deficits.

Results

Normal neurological functions in $APP^{YG/YG}$ mice

Visual inspection did not reveal obvious difference between $APP^{WT/WT}$ and $APP^{YG/YG}$ mice. $APP^{YG/YG}$ mice maintained a normal gait and posture and no abnormal stereotyped behaviors or signs of ataxia or dystonia were observed. Eyes were normally open and lacrimation was absent. Fur appeared tidy and well groomed, piloerection was absent, and whiskers were intact in all mice. Righting reflex showed comparable results for the two genotypes (data not shown). Mice were weighed monthly until 7 month of age. No differences between $APP^{YG/YG}$ and $APP^{WT/WT}$ mice were detected in the growth curve (Fig. 1A).

$APP^{YG/YG}$ mice present altered neuromuscular and physical performances, reduced paired-pulse ratio, and increased synaptic failure

To search for possible abnormalities in muscular strength, we performed the hang wire test in young and adult $APP^{WT/WT}$ and $APP^{YG/YG}$ mice. Latencies to fall in hanging wire test were similar in 2-month-old $APP^{WT/WT}$ and $APP^{YG/YG}$ mice, while it was significantly reduced in 5-month-old $APP^{YG/YG}$ mice (Fig. 1B).

Two-month-old $APP^{WT/WT}$ and $APP^{YG/YG}$ mice showed similar locomotor activity, as measured by the number of crossings during 60 min of free exploration in shuttle-box cages (Fig. 1C). At 5 month of age, $APP^{WT/WT}$ mice showed a significantly reduced locomotor activity than that at 2 month of age, while 5-month-old $APP^{YG/YG}$ mice were significantly more active compared to age-matched WT mice (Fig. 1C).

To test for possible motor coordination impairments, we performed rotarod test at accelerated rate. Rotarod test was preceded by few trials of training in which mice were habituated to stay in equilibrium on the rod at fixed rate. Figure 1D shows the mean rotarod performances, recorded in $APP^{WT/WT}$ and $APP^{YG/YG}$ mice at 2 month (left panel) and 5 month (right E) of age, expressed as mean time on the rod before falling during both the four trials of training (trials 1–4) with rotarod at fixed rate and the eight trials of testing (trials 5–12) with accelerated rotarod. Interestingly, during the training phase, $APP^{YG/YG}$ mice learned less quickly than $APP^{WT/WT}$ mice to stay in equilibrium in the rod rotating at fixed speed. This is particular evident in 5-month-old $APP^{YG/YG}$ mice. RMANOVA showed no significant differences in mice at 2 month of age ($F_{1,14} = 2.996$; $P = 0.1055$) and confirmed significant difference between the two genotypes at 5 month of age during training phase (trials 1–4) with significant main effect for genotypes ($F_{1,13} = 8.806$; $P = 0.0109$), for trials ($F_{3,33} = 8.947$; $P = 0.0001$), and significant genotypes × trials interaction ($F_{3,33} = 4.625$; $P = 0.0073$). *Post hoc* comparison showed significant differences between $APP^{YG/YG}$ mice and $APP^{WT/WT}$ during training at trials 1–3. Although $APP^{YG/YG}$ mice showed an impairment initially, at the end of training phase, that is, at trial 4, $APP^{YG/YG}$ mice reached the same performance of $APP^{WT/WT}$ mice. During testing phase, with rod rotating at accelerated speed, $APP^{WT/WT}$ and $APP^{YG/YG}$ mice behaved almost identical, without significant differences at both 2 and 5 month of age (RMANOVA; 2 month: $F_{1,14} = 0.363$; $P = 0.5562$; 5 month: $F_{1,13} = 0.009$; $P = 0.9254$).

By means of accelerated treadmill, we tested the physical resistance of mice during an endurance exercise. Figure 1E–G shows that 2-month-old mice behaved similarly in total running time, total distance, and work performed. However, at 5 month of age, $APP^{YG/YG}$ mice showed a significant reduction in total running time, total distance, and vertical work performed.

To determine whether abnormal neuromuscular transmission is correlated with altered motor function seen in $APP^{YG/YG}$ mice, we evaluated endplate potential (EPP) in diaphragms of 5-month-old $APP^{WT/WT}$ and $APP^{YG/YG}$ mice. We first compared single electrical stimulation-induced EPP, and the $APP^{YG/YG}$ EPP showed similar amplitude compared to controls ($APP^{WT/WT}$: 8.8 ± 0.7, $N = 19$; $APP^{YG/YG}$: 8.5 ± 1.04, $N = 20$). We next performed paired-pulse protocol by applying two stimulating pulses at 20-, 50-, 100-, and 200-ms intervals in control and $APP^{YG/YG}$ NMJs. A significantly lower ($P < 0.05$) paired-pulse ratio was observed in $APP^{YG/YG}$ diaphragm at interpulse intervals of 20 and 50 ms (Fig. 1H), which is similar to what have been seen in $APP^{-/-}$ mouse model, although the latter demonstrated more severe deficits (Yang *et al.*, 2007). We then tested the response of $APP^{YG/YG}$ NMJs to 1-s stimulus training at 50, 100, and 200 Hz. Synaptic failure was observed at high frequency (200 Hz) in five of ten recordings in $APP^{YG/YG}$ mice, which was two of 13 in $APP^{WT/WT}$ mice (Fig. 1I).

Altogether, the results show that, compared to WT mice, $APP^{YG/YG}$ mice are normal in locomotor activity and motor coordination but develop impairment in physical resistance and a reduced neuromuscular strength.

Altered cognitive performances of $APP^{YG/YG}$ mice

To test the ability of learning and memory in $APP^{YG/YG}$ mice during learning of conditioned task, we performed the active avoidance (AA) test. AA represents a behavioral paradigm to evaluate the associative learning and the retention of conditioning events. Figure 2A,B shows the avoidance responses during 5 days of 100-trial AA sessions in $APP^{YG/YG}$ and $APP^{WT/WT}$ mice at 4 and 7 month of age. As previously reported (Bovet *et al.*, 1969), C57BL/6J mice learned this task quite poorly. In fact, only 30% and 45% of AA were recorded at 4 and 7 month of age, respectively. A completely different behavior was observed in $APP^{YG/YG}$ mice. At 4 months of age, these mice appeared to learn more rapidly to avoid electric shock than $APP^{WT/WT}$ mice during the fifth session (Fig. 2A). In contrast, at 7 month of age, the $APP^{YG/YG}$ mice were significantly impaired during sessions 4 and 5, compared to WT mice (Fig. 2B). RMANOVA of the avoidance responses of 4-month-old mice showed that there was no significant effect for genotype ($F_{1,20} = 1.911$; $P = 0.1821$), but a significant effect of daily session ($F_{4,40} = 39.415$; $P < 0.0001$) and a significant genotype × session interaction ($F_{4,80} = 2.818$; $P = 0.0305$). In 7-month-old mice, we found a main effect for genotype ($F_{1,20} = 14.810$; $P = 0.001$), for avoidance session ($F_{4,40} = 69{,}103$; $P < 0.0001$), and for genotype × avoidance session interaction ($F_{4,80} = 11.952$; $P < 0.0001$). *Post hoc* comparison showed significant differences between $APP^{YG/YG}$ and $APP^{WT/WT}$ mice only during session 5 at 4 month of age (improved learning) and during sessions 4 and 5 at 7 month of age (impaired learning).

To further test the memory, we performed novel object recognition (NOR) and radial-arm water maze (RAWM) tests. NOR is a nonaversive task that relies on the mouse's natural exploratory behavior. Open field studies showed that $APP^{WT/WT}$, $APP^{YG/WT}$, and $APP^{YG/YG}$ mice have no defects in habituation, locomotor, and anxiety-like behavior (Fig. 2C,D). Mice were analyzed at 4, 5, 8, and 13 month of age. At all ages, mice of all genotypes spent the same amount of time exploring the two identical objects during the training session (Fig. 2E,G,I,K). At 4 month of age, when a novel object was introduced the following day, $APP^{WT/WT}$,

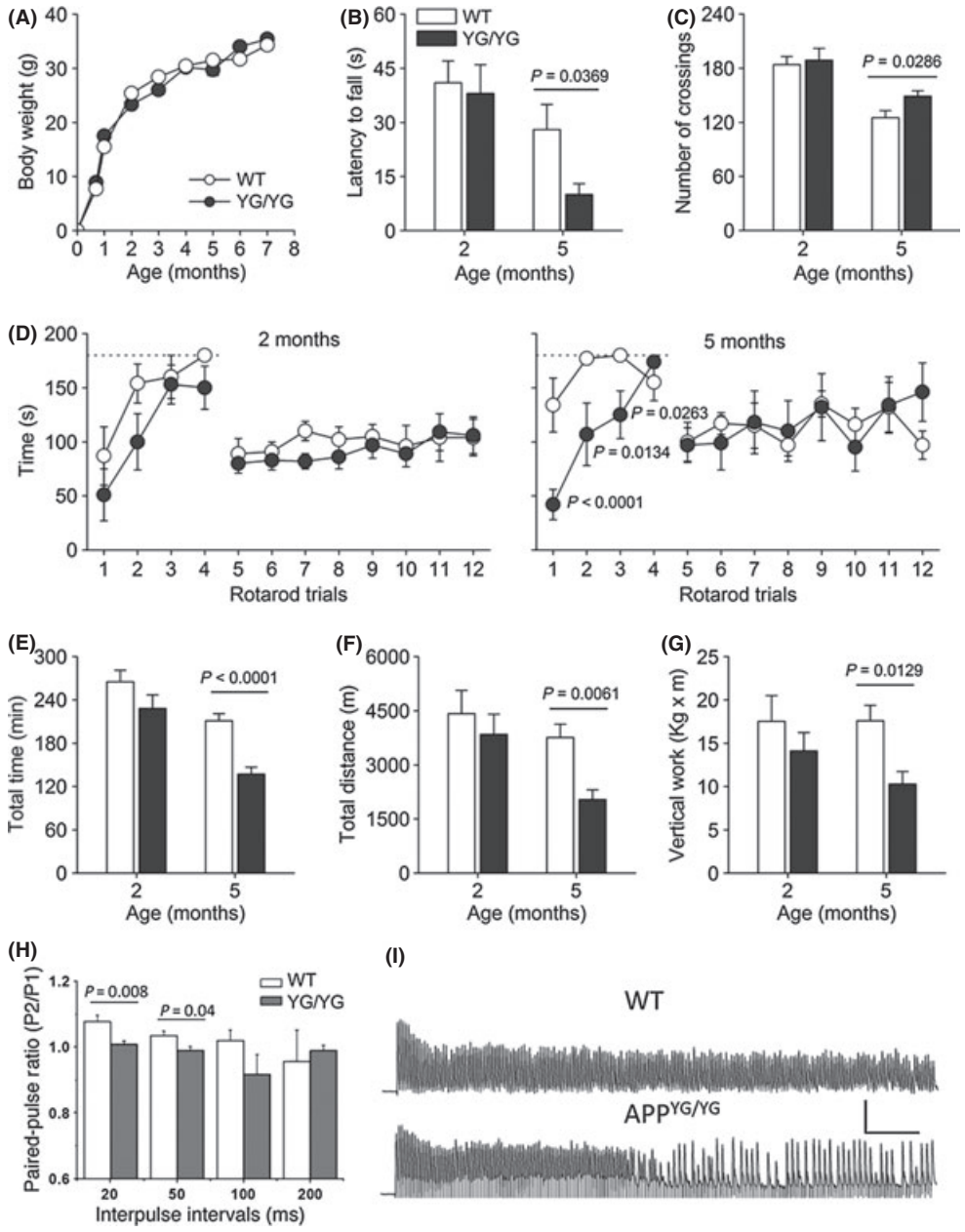

Fig. 1 Behavioral characterization and paired-pulse and 200-Hz training stimulation–induced EPPs in NMJs of $APP^{YG/YG}$(YG) and $APP^{WT/WT}$(WT). The different panels represent (A), growth curves from weaning to 7 month of age; (B), latency to fall in hanging wire; (C), locomotor activity, measured as the number of crossings in shuttle-box cages; (D), time to fall from rotarod during training and testing trials; (E), total time of running during the whole treadmill running; (F), total distance travelled during treadmill running; and (G), vertical work performed during treadmill running. Dashed line in panel D indicates cutoff time, set at 180 s, during the rotarod training trials. The number of mice was 8–10 for each genotype, except for panel A where the number of mice was 15–17. Data were analyzed by Student's *t*-test, except for data in panel D which were analyzed by two-factor RMANOVA followed by *post hoc* pairwise comparison using Bonferroni–Dunn test. (H) Summary of paired-pulse ratio (P2/P1) in $APP^{YG/YG}$ ($N = 16$) and $APP^{WT/WT}$ ($N = 21$) at various interpulse intervals. (I) Representative traces showing 200-Hz training stimulation–induced responses in $APP^{YG/YG}$ and $APP^{WT/WT}$ NMJs. Scale: 5 mV, 100 ms. APP, Aβ-precursor protein; EPP, endplate potential.

$APP^{YG/WT}$, and $APP^{YG/YG}$ mice spent more time exploring the novel object (Fig. 2F). However, 5-month-old $APP^{YG/YG}$ mice spent the same amount of time exploring the two objects as if they were both novel to them, while $APP^{YG/WT}$ mice behaved like the $APP^{WT/WT}$ and explored preferentially the novel object (Fig. 2H). At 8 and 13 month of age, both $APP^{YG/WT}$ and $APP^{YG/YG}$ mice showed NOR memory deficits (Fig. 2J,L), showing that the APP^{YG} mutation causes severe aging- and dose of mutation-dependent memory deficits.

We performed the spatial working memory test RAWM, which depends upon hippocampal function and tests short-term memory. Mice were required to learn and memorize the location of a hidden platform in one of the arms of a maze with respect to spatial cues. At

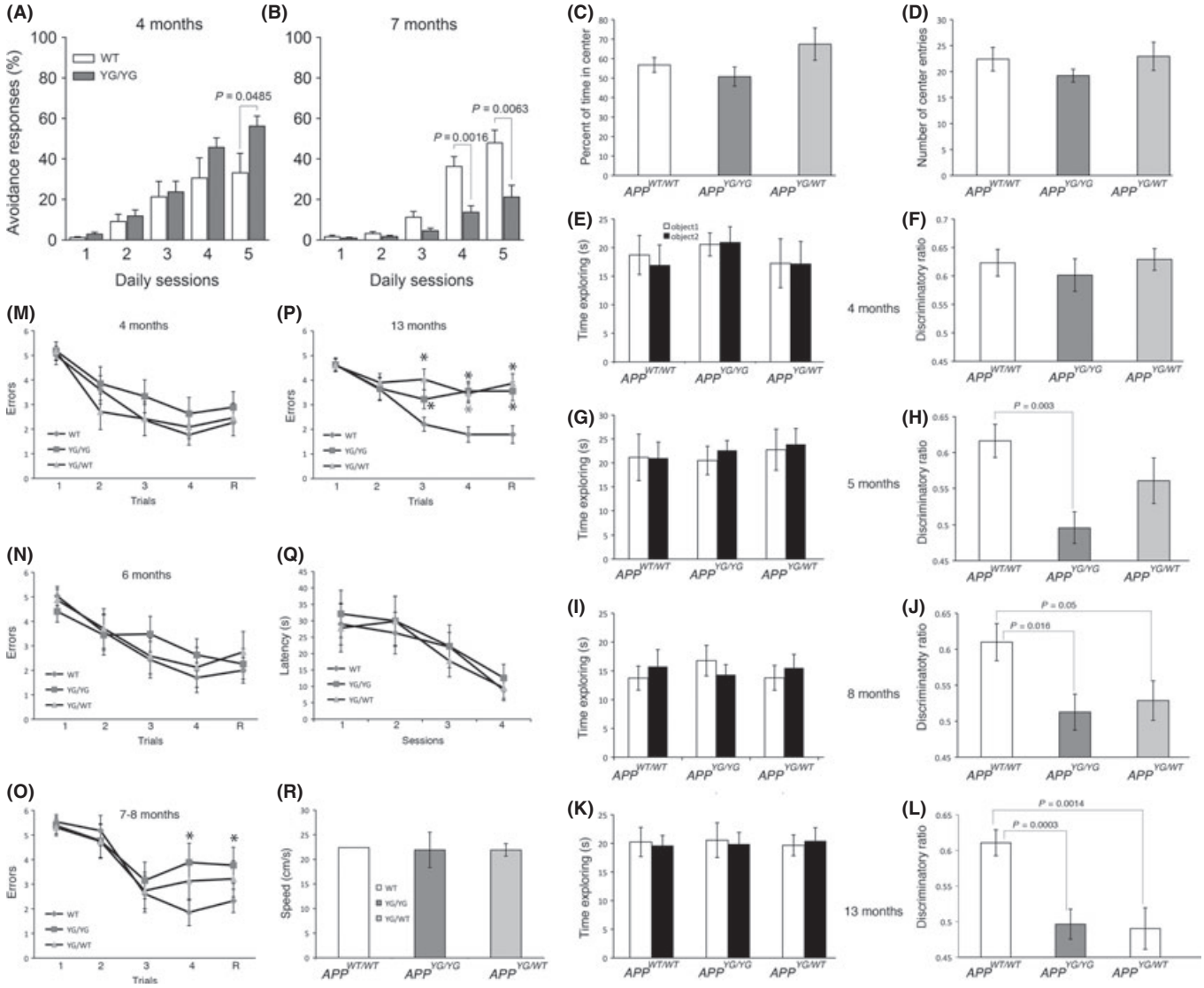

Fig. 2 *APP*$^{YG/WT}$ and *APP*$^{YG/YG}$ mice develop age-dependent memory impairments. (A,B) AA behavioral responses, calculated as cumulative number of shock avoidance during 100 trials over 5 days in *APP*$^{WT/WT}$ (WT) and *APP*$^{YG/YG}$ (YG/YG) mice at 4 and 7 month of age. The number of mice was 8 for each genotype–age group. Statistical analysis: RMANOVA followed by *post hoc* pairwise comparison between WT and YG/YG mice, at 4 and 7 months of age, using Bonferroni–Dunn test. (C,D) Open field is a sensorimotor test for habituation, exploratory, emotional behavior, and anxiety-like behavior, in novel environments. The percent of time in center (C) and the number of entries into the center (D) are indicators of anxiety levels. The more the mouse enters the center and explores it, the lower the level of anxiety-like behavior. Because the *APP*$^{YG/WT}$ and *APP*$^{YG/YG}$ mice are similar to the WT mice, there is no deficit or excess of anxiety. (E,F) Four-month-old *APP*$^{YG/WT}$ and *APP*$^{YG/YG}$ mice have normal object recognition memory. After spending the same amount of time exploring the two identical objects on day 1 (E), the 4-month-old *APP*$^{WT/WT}$, *APP*$^{YG/WT}$, and *APP*$^{YG/YG}$ male mice spent more time exploring the novel object 24 h later (F), showing normal object recognition. (G–L) *APP*$^{YG/WT}$ and *APP*$^{YG/YG}$ mice show a progressive loss of object recognition memory as they age, which becomes first detectable at 5 month of age for *APP*$^{YG/YG}$ mice and at 8 month of age for *APP*$^{YG/WT}$ mice. (M–P) *APP*$^{WT/WT}$, *APP*$^{YG/WT}$, and *APP*$^{YG/YG}$ male mice were run through a RAWM task, testing spatial working memory. At 4 and 6 month of age, *APP*$^{YG/WT}$ and *APP*$^{YG/YG}$ mice made a similar number of mistakes compared to their WT littermates (M,N). (O) At 7–8 month, *APP*$^{YG/YG}$ mice showed spatial working memory deficits in the fourth acquisition (A4, *APP*$^{WT/WT}$ vs. *APP*$^{YG/YG}$, $P = 0.0004$) and the retention (R, *APP*$^{WT/WT}$ vs. *APP*$^{YG/YG}$, $P = 0.010$) trials. (P) At 13 month of age, both *APP*$^{YG/WT}$ and *APP*$^{YG/YG}$ mice showed short memory deficits in both acquisition and retention trial (A3, *APP*$^{WT/WT}$ vs. *APP*$^{YG/YG}$, $P = 0.034$; A4, *APP*$^{WT/WT}$ vs. *APP*$^{YG/YG}$, $P = 0.0008$; R, *APP*$^{WT/WT}$ vs. *APP*$^{YG/YG}$, $P = 0.0012$; A3, *APP*$^{WT/WT}$ vs. *APP*$^{YG/WT}$, $P = 0.0004$; A4, *APP*$^{WT/WT}$ vs. *APP*$^{YG/WT}$, $P = 0.0005$, R, *APP*$^{WT/WT}$ vs. *APP*$^{YG/WT}$, $P = 0.0002$). (Q,R) *APP*$^{WT/WT}$, *APP*$^{YG/WT}$ and *APP*$^{YG/YG}$ mice need similar time (latency) and have similar speed (speed) to reach a visible platform. APP, Aβ-precursor protein; RAWM, radial-arm water maze.

4 and 6 month of age, *APP*$^{WT/WT}$, *APP*$^{YG/WT}$, and *APP*$^{YG/YG}$ mice were able to acquire (A) and retain (R) memory of the task (Fig. 2M,N). Seven- to eight-month-old *APP*$^{YG/YG}$ mice showed abnormalities during both acquisition and retention of the task (Fig. 2O), and at 13 month of age, both *APP*$^{YG/WT}$ and *APP*$^{YG/YG}$ mice showed severe impairment in short-term spatial memory for platform location during both acquisition and retention of the task (Fig. 2P). This defect was due to a deficit in memory *per se* and not to deficits in vision, motor coordination, or motivation because testing with the visible platform showed no difference in the time needed to find the platform and swimming speed between the *APP*$^{WT/WT}$, *APP*$^{YG/WT}$, and *APP*$^{YG/YG}$ mice (Fig. 2Q,R). Taken together, these findings provide compelling genetic evidence that Y^{682} of APP plays an important function in normal memory formation.

Region-specific and age-dependent dendritic spine loss in *APP$^{YG/YG}$* mice

Synaptic loss correlates with cognitive impairment (Arendt, 2009). Dendritic spines, the protrusions emerging from the dendritic shaft of neurons, are the primary sites of excitatory synapses, and their density reflects the synaptic connectivity of the neural circuits they belong to. Accordingly, the impact of the $Y^{682}G$ mutation on dendritic spine density was analyzed in Golgi-stained CA1 pyramidal hippocampal and spiny dorsolateral striatal (DSL) neurons involved in cognitive and motor learning, respectively. The ANOVA performed on hippocampal spines (Fig. 3) counted in the apical dendrite compartment revealed a significant main effect of genotype ($F_{1,101} = 60.63$; $P < 0.001$), of age ($F_{1,101} = 5.126$; $P < 0.05$), and a significant genotype × age interaction ($F_{1,101} = 9.30$; $P < 0.01$). *Post hoc* comparisons showed that spine density was significantly lower in *APP$^{YG/YG}$* mice than in *APP$^{WT/WT}$* mice at both age-points ($P < 0.01$). Importantly, although spine density was stable across age-points in the *APP$^{WT/WT}$* mice ($P > 0.05$), it was significantly lower in 7-month-old than in 2-month-old mutants ($P < 0.001$), thus indicating a mutation-specific age-dependent spine loss. The ANOVA performed on hippocampal spines counted in the basal dendrite compartment also revealed a significant main effect of genotype ($F_{1,162} = 162.6$; $P < 0.001$), of age ($F_{1,162} = 28.61$; $P < 0.001$), but no significant genotype × age interaction ($F_{1,162} = 1.47$; $P > 0.1$). Thus, different from what observed for apical dendrites, age-dependent spine loss was evident in both genotypes, although it was considerably stronger in *APP$^{YG/YG}$* mutants. The ANOVA performed on DSL spines (Fig. 3) also showed a main effect of genotype ($F_{1,118} = 60.23$; $P < 0.001$), of age ($F_{1,118} = 6.270$; $P < 0.05$), but no significant genotype × age interaction. As for hippocampal basal dendrites, less spines were counted on DSL neurons of *APP$^{YG/YG}$* at each age-point, therefore revealing that spine density decreased with age in both genotypes, this effect being more marked in *APP$^{YG/YG}$* mice than in *APP$^{WT/WT}$* mice. Altogether, our data provide the evidence that the Y^{682} mutation severely disrupts the connectivity in hippocampal and DLS circuits.

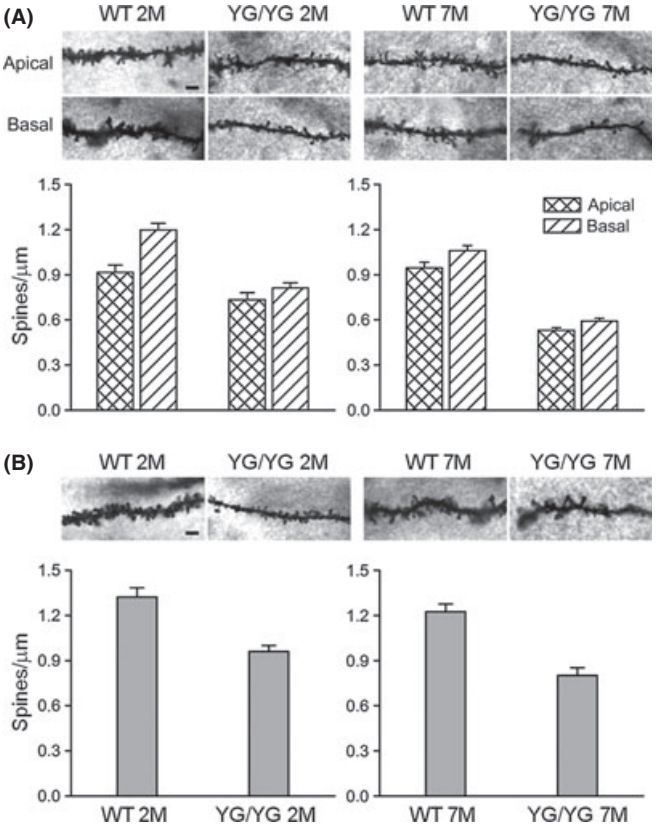

Fig. 3 Aging-dependent reduction in dendritic spine density in *APP$^{YG/YG}$* mice. (A-top) Representative examples of photomicrographs of Golgi-Cox-stained dendritic segments of CA1 pyramidal neurons (apical and basal compartment) in 2- and 7-month-old *APP$^{WT/WT}$* (WT 2 month; WT 7 month) and *APP$^{YG/YG}$* (YG/YG 2 month; YG/YG 7 month) mice, respectively. Magnification: 100 × 1.25 NA. Scale bar: 3 μm. (A-bottom) Effects of genotype on dendritic spine density measured on CA1 pyramidal neuron in basal and apical compartments in 2- and 7-month-old *APP$^{WT/WT}$* and *APP$^{YG/YG}$* mice. (B-top) Representative examples of photomicrographs of Golgi-Cox-stained dendritic segments of dorsolateral striatum spiny neuron dendrites in 2- and 7-month-old *APP$^{WT/WT}$* and *APP$^{YG/YG}$* mice. Magnification: 100 × 1.25 NA, Scale bar: 3 μm. (B-bottom) Effects of genotype on dendritic spine density measured on dorsolateral striatum spiny neuron dendrites in 2- and 7-month-old *APP$^{WT/WT}$* and *APP$^{YG/YG}$* mice. APP, Aβ-precursor protein.

Reduced expression levels of ChAT and TrkA proteins in brain from *APP$^{YG/YG}$* mice

Several data indicate a correlation between muscular functions and cholinergic tone (Schliebs & Arendt, 2011). Cholinergic neurons in the CNS undergo complex changes during normal aging, leading to a reduced support of NGF via TrkA/p75 receptors (Niewiadomska *et al.*, 2011; Schliebs & Arendt, 2011), and deficit in NGF signaling causes atrophy and loss of cholinergic neurons (Ruberti *et al.*, 2000). These data and the evidence showing impaired NGF/TrkA signaling in *APP$^{YG/YG}$* mice (Matrone *et al.*, 2011) prompted us to analyze the expression levels of choline acetyltransferase (ChAT) and TrkA proteins in different brain structures, such as hippocampus (Hp), striatum (Str), cortex (Cx), and septum (Spt). *APP$^{YG/YG}$* mice show a progressive reduction in the expression levels of ChAT and TrkA in Hp and Spt. TrkA, but not ChAT expression, was decreased also in striatum of *APP$^{YG/YG}$* mice. Neither protein was reduced in the Cx. Such reductions reached the peak at 6 month of age (Fig. 4A,B,E). Consistent with the WB analysis, a significant reduction in the number of ChAT-positive neurons was observed in the hippocampus, septum, and caudate of 6-month-old *APP$^{YG/YG}$* mice (Fig. 4C,D). Furthermore, the reduction in the expression of ChAT protein and the significant loss of the cholinergic stained nuclei are associated with the decrease in the septum volume (Fig. 4D), indicative of cholinergic tone impairment in such area. Conversely, the hippocampus and caudate volumes are not affected.

Discussion

A role of Y^{682} of APP in development was previously reported. Mutation of Y^{682} into a G alters APP trafficking and processing leading to a redistribution of APP toward the nonamyloidogenic pathway (Barbagallo *et al.*, 2010). Moreover, Y^{682} plays a fundamental role in the functions of APP necessary for normal development as shown by the evidence that *APP$^{YG/YG}$/APLP2$^{-/-}$* mice present with postnatal lethality and neuromuscular synapse defects similar to doubly deficient *APP/APLP2* mice (Barbagallo *et al.*, 2011). Thus, Y^{682} is indispensable for the essential function of APP in developmental regulation. Additionally, an intimate crosstalk between APP and NGF pathways has been described, and Y^{682} plays a central role in this functional relationship (Matrone *et al.*, 2008, 2009, 2011; Calissano *et al.*, 2010).

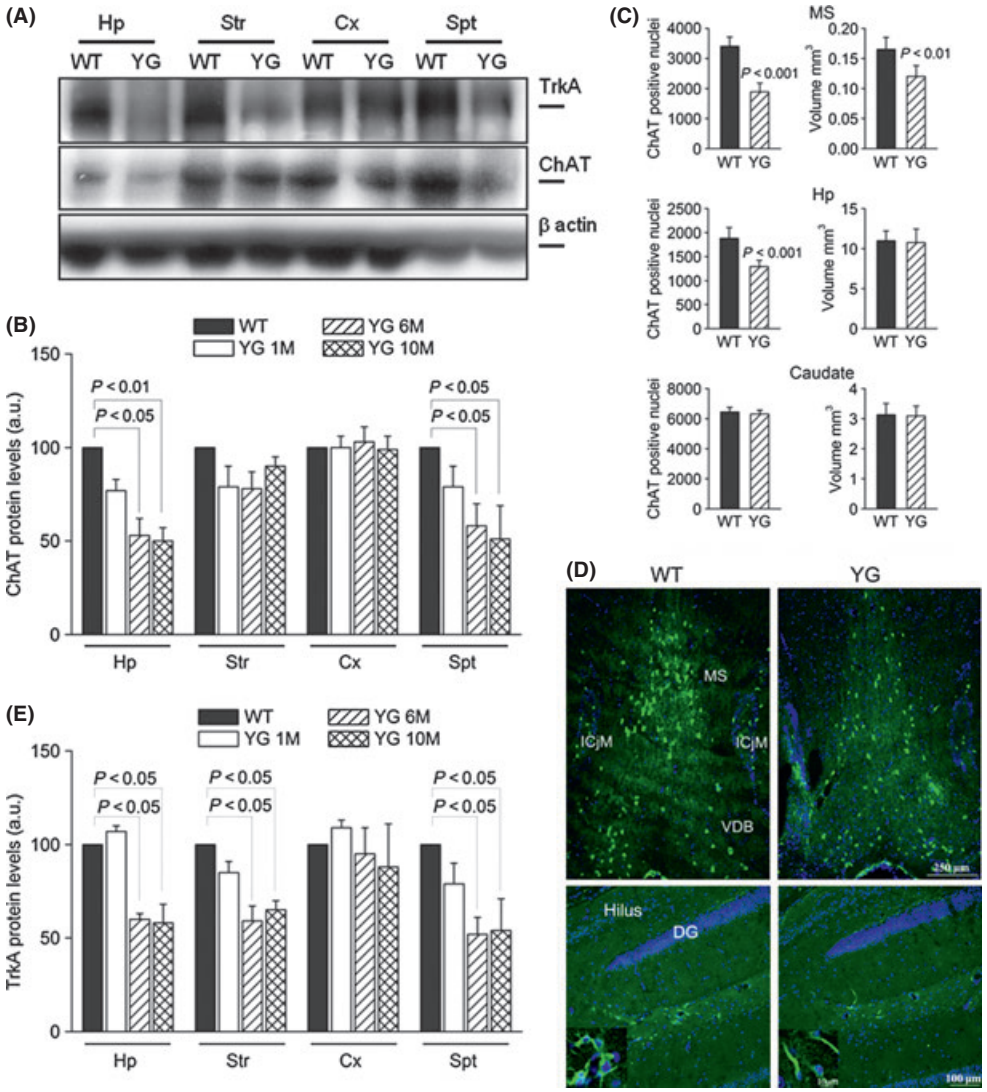

Fig. 4 Aging-dependent ChAT and TrkA expression levels in dissected brain areas from $APP^{YG/YG}$ (YG) and $APP^{WT/WT}$ (WT) mice. (A) Western blots performed in cortex (Cx), hippocampus (Hp), septum (Spt), and striatum (Str) from 1-, 6-, and 10-month-old mice. Optical density (OD) analysis for ChAT ($N = 4$) and for TrkA ($N = 6$) proteins was reported in panels (B) and (E), respectively. Data were normalized on the basis of the corresponding β-actin values and expressed as% of WT ($N = 7$; Newman–Keuls test) WT. a.u. (arbitrary unit). (C) Number of ChAT-positive nuclei and volume of different brain areas from 6-month-old mice. Representative pictures of ChAT-positive nuclei (green) in septum and hippocampus were reported in panel (D). Abbreviations: MS, Medial Septum; ICjM, islands of Calleja-Major; VDB, Vertical Diagonal Band; DG, Dentate Gyrus; APP, Aβ-precursor protein.

Here, we show that APP regulates neuronal homeostasis and aging via Y^{682}. The $APPY^{682}G$ mutation causes an aging-dependent neuronal decline, leading to aging-dependent reduction in (i) muscular strength; (ii) physical performance during treadmill protocol of endurance exercise; (iii) motor learning performance; (iv) AA learning; (v) object recognition and short-term spatial working memory; (vi) hippocampal and DSL synaptic connectivity; (vii) cholinergic tone and TrkA levels in hippocampus and septum.

$APP^{YG/YG}$ mutant mice do not have motor coordination deficit but are less vigorous and more prone to fatigue than $APP^{WT/WT}$ mice already at 5 month of age. This is probably due to reduced neuromuscular strength as suggested by EPP data. Interestingly, $APP^{YG/YG}$ mice also develop aging-dependent learning and memory deficits. Active avoidance test shows a cognitive decline in 7-month-old $APP^{YG/YG}$ mice, which is similar to that observed in 10-month-old $APP^{-/-}$ mice (Dawson *et al.*, 1999). $APP^{YG/YG}$ and $APP^{YG/WT}$ mice also develop aging-dependent deficits in object recognition and spatial working memory. Consistent with the poor cognitive and motor performance, $APP^{YG/YG}$ mice showed massive synaptic loss in the hippocampus, which controls spatial working memory and long-term object recognition (D'Amato *et al.*, 2011), and in the DSL, which, apart from its role in motor functions, is selectively involved in AA learning (Ammassari-Teule *et al.*, 2009). Interestingly, spine loss was already evident at 2 month of age, when $APP^{YG/YG}$ mice do not yet show behavioral impairments, suggesting that a critical synaptic loss threshold has to be reached before cognitive and motor functions are altered and that synaptic loss precedes behavioral deficits.

Aβ-precursor protein (APP) transgenic mice, which are widely used as animal models of AD, develop memory deficits similar to those seen in $APP^{YG/YG}$ animals. The memory deficits of APP transgenic mice are attributed to increased production of Aβ and amyloid burden. However,

$APP^{YG/YG}$ mice show a significant decrease in Aβ levels (Barbagallo *et al.*, 2010), suggesting that alterations in APP function/processing can lead to memory deficits that are not linked to Aβ. Whether similar mechanisms can also lead to aging-dependent forms of dementias without amyloidosis in humans remains to be determined.

Although it is tempting to speculate that the compromised crosstalk between NGF/TrkA signaling and APP processing is mechanistically linked to the decline in cholinergic tone, cognitive and neuromuscular performance of $APP^{YG/YG}$ mice, further experiments will be needed to establish direct cause–effect relationships among these deficits. Nevertheless, the profound deficits caused by this single point mutation of APP indicate that $APP^{YG/YG}$ mice can be useful to dissect the mechanistic aspects of APP function in physiological and pathological processes.

Experimental procedures

Preliminary observation

The animals used for these studies were backcrossed to C57Bl6/J mice for at least 14 generations. Mice were handled according to NIH and Italian ethical regulations. $APP^{YG/YG}$ mice were used in all the experiment with C57BL/6J mice serving as WT controls. For NOR and RAWM, $APP^{YG/YG}$, $APP^{YG/WT}$, and $APP^{WT/WT}$ mice used were littermates derived from crossings of male and female $APP^{YG/WT}$ mice. For preliminary observations and behavioral assessment, 8–10 $APP^{WT/WT}$ and $APP^{YG/YG}$ were tested. Sequence of behavioral examinations was as follows: At day 1, mice were subjected to preliminary neurological screening and to tail-suspension and righting reflex tests; after 1 day of rest, at day 3, mice were subjected to locomotor activity followed again by 1 day of rest; at day 5, mice begun treadmill running test which was protracted for 9 days with 1 day of rest between each running sessions; finally, starting from day 23, mice performed 7 days of rotarod test. All testing were carried out blindly. Gait and posture, tremors, palpebral closure and lacrimation, piloerection and whisker appearance, grooming and defecation were taken as indexes of general health status. Visual inspection was performed by putting mouse into a white plastic sheet surrounded by a clear acrylic cylindrical viewing jar (14 cm diameter; 18 cm height) and observing mouse behavior for 5 min. After 5-min observation, mice were subjected to righting reflex. Turning the mouse on its back and recording the latency to regain the footing position from the back position evaluated righting reflex.

Assays of neuromotor behavior

Hang wire test

Neuromuscular strength was tested by hang wire test. For this purpose, mice were placed on a steel bar (55 cm length; 2 mm thick) and the ability to hold in equilibrium on the bar with their forelimb/hind limb was measured as latency to fall off a wire after exhaustion. A cutoff time of 60 s was considered as the end of test.

Locomotor activity test

Locomotor activity was tested in eight toggle-floor cages. Each cage consisted of a rectangular white 40 × 10 cm Plexiglas box divided into two equal 20 × 10 cm compartments by a 3 × 3 cm opening through a black partition. The number of crossings from one side of the box to the other was recorded automatically by means of a micro-switch connected to the tilting floor of the box. Mice were subjected to a 60-min activity test and the number of crossings between the two compartments represented the score for each mouse (Luvisetto *et al.*, 2004).

Rotarod, which tests motor coordination, balance, and motor learning ability, was performed in three phases, as reported (Luvisetto *et al.*, 2008): habituation (1 day), training (2 days), and testing (4 days). The mice were subjected to two daily trials separated by a 45-min interval. Mice were accustomed to the stationary rod (habituation) and to the rod rotating at 6 rpm (training) for 3 min. During the four consecutive days of testing, mice were placed on the rod rotating at 4 rpm for 30 s, after which acceleration was started and gradually increased to 40 rpm over a time course of 5 min. Testing sessions were terminated after 5 min or when mice fell off the rod.

Treadmill running exercise

Exercise studies were performed on five-lane motorized treadmill equipped with an electronic control unit and an electric shock grid at one end of the treadmill. Shock intensity was set at 0.4 mA. Inclination of treadmill was set at 8.5° (15%). Mice were subjected to an endurance protocol with treadmill belt running at incremental speed. Exercise was repeated for 9 days with 1 day of rest between each trial. At each day, mice were first acclimated with treadmill for 1 min, followed by a running session with belt speed initially set at 15 m min^{-1}. After 10 min, belt speed was increased by 3 m min^{-1} every 5 min and exercise continued until exhaustion. Exhaustion was considered as inability to maintain running speed despite repeated contact with the electric grid. The time for the removal of mice from the treadmill was 5 s on the shocker plate without attempting to reengage the treadmill. The time to exhaustion and whole travelled distance were automatically recorded from the beginning of the running session. Endurance exercise performances were estimated by the time of running (in min), the travelled distance (in m), and the vertical work (in kg × m) performed by each mouse. Then, for each animal, daily parameters were summed and the cumulative values after nine trials were averaged for the different genotype–age mice groups. According to Massett & Berk (2005), vertical work was calculated as the product of body weight (in kg) and vertical distance (in m), where vertical distance was the product between travelled distance and sin (α), where α is equal to angle of treadmill inclination.

Cognitive tests

AA acquisition

The same apparatus employed to measure locomotor activity was used for the measurement of AA acquisition. The apparatus was computer controlled and consisted of eight shuttle-boxes; each one divided into two-20 × 10 cm compartments, connected by a 3 × 3 cm opening. A light (10W) was switched on alternately in the two compartments and used as a conditioned stimulus (CS). The CS preceded the onset of the unconditioned stimulus (US) by 5 s and overlapped it for 25 s. Using this procedure, the light was present in the compartment for 30 s: 5 s alone and 25 s together with the US. At the end of the 30-s period, both CS and US were terminated automatically, and the cycle began in the other compartment. The US was an electric shock (0.2 mA) applied continuously to the grid floor. An avoidance response was recorded when the animal avoided the US by running into the dark compartment within 5 s after the onset of the CS. If animals failed to avoid the shock, they could escape it by running from the US. Failure of either avoidance or escape response seldom occurred. Mice were subjected to five daily 100-trial avoidance sessions.

Spatial working memory

The task studied with the RAWM test has been described previously (Tamayev *et al.*, 2011). The scores for each mouse on the last 3 days of testing were averaged and used for statistical analysis. Briefly, a six-armed maze was placed into white tank filled with water (24–25 °C) and made opaque by the addition of nontoxic white paint. Spatial cues were presented on the walls of the testing room. At the end of one of the arms was positioned a clear 10 cm submerged platform that remained in the same location for every trial in 1 day but was moved approximately randomly from day to day. On each trial, the mouse started the task from a different randomly chosen arm. Each trial lasted 1 min, and errors were counted each time the mouse entered the wrong arm or needed more than 10 s to reach the platform. After each error, the mouse was pulled back to its starting position. After four consecutive acquisition trials, the mouse was placed in its home cage for 30 min, then returned to the maze, and administered a fifth retention trial.

Visible platform testing

Visible platform testing to assess; visual and motor deficits was performed in the same pool as in the RAWM; however, the arms of the maze were removed. The platform was marked with a black flag and positioned randomly from trial to trial. Time to reach the platform and speed were recorded with a video tracking system (HVS 2020; HVS Image, UK).

Open field and NOR

After 30 min to acclimate to the testing room, each mouse was placed into a 40 × 40 cm open field chamber with 2-ft-high opaque walls. Each mouse was allowed to habituate to the normal open field box for 10 min, and repeated again 24 h later, in which the video tracking system (HVS 2020; HVS Image) quantifies the number of entries into and time spent in the center of the locomotor arena. NOR was performed as previously described (Taglialatela *et al.*, 2009). The results were recorded as discrimination ratio, which is calculated by dividing the time the mice spent exploring the novel object by the total amount of time exploring the two objects.

Statistical analysis of behavioral data

All data are shown as mean ± SEM. Data for growth curves, hanging wire and locomotor activity, as well as for total time, total distance, and work performed during treadmill test, were analyzed using Student's *t*-test. Statistics for NOR and RAWM tests were performed by one-way analysis of variance (ANOVA). Statistics for rotarod, daily treadmill running, and active avoidance tests were performed by two-factor analysis of variance for repeated-measures ANOVA (RMANOVA), considering genotype and age group as between-subject factor and daily sessions as within-subject factor. When appropriate, pairwise comparisons between genotype and age groups were made using Bonferroni–Dunn test.

Spine density analysis

Golgi-Cox staining

$APP^{YG/YG}$ mice (2 months, $N = 5$; 7 months, $N = 5$) and WT mice (2 months old $n = 4$; 7 months old $n = 5$) were sacrificed via transcardially perfusion with 200 ml 0.9% saline solution under deep anesthesia (chloral hydrate 400 mg kg^{-1}). Brains were dissected and the two hemispheres were impregnated separately in a Golgi-Cox solution (1% potassium dichromate, 1% mercuric chloride, 0.8% potassium chromate) at room temperature. Samples were then placed in sucrose (30%) for 3 days, sectioned coronally (100 μm) using a vibratome, and mounted. The color reaction consists of consecutive steps in water (10 min), ammonium hydroxide (30 min), water (10 min), the developer solution (Kodak fix 100%, 30 min), and water (10 min). Sections were then dehydrated through successive steps in alcohol at increasing concentrations (50%, 75%, 95%, and 100%) before being closed with slide cover slips. All successive measurements were taken by an investigator blind to the experimental condition of the sample under examination.

Quantification of spine density

Hippocampal CA1 pyramidal or DLS spiny neurons were identified under low magnification (20X 0.5 NA) using an optical microscope DMLB Leika (Leica Microsystems, Wetzlar, Germany). Subsequently, dendritic spines were quantified online at a magnification of 100 × 1.5 NA using a camera (Qicam Fast1394; Qimaging, Surrey, BC, Canada) connected to the microscope. Spine density was measured on the apical and basal dendrites of hippocampal CA1 pyramidal neurons. Measurements were taken on segments of CA1 basal dendrites (secondary, tertiary, and quaternary branches), of CA1 apical dendrites (secondary and tertiary branches), and of DLS spiny neuron dendrites (secondary and tertiary branches); all data were analyzed using the software Neurolucida. Data collected in each brain region were analyzed by means of two-way ANOVAs with genotype and age-point as main factors. Bonferroni *post hoc* tests were then used for pairwise comparisons where necessary.

Immunofluorescence analysis

Tissue processing and IHC were performed in free-floating sections. Briefly, mice were anesthetized with 400 mg kg^{-1} choral hydrate (Sigma Aldrich, Rome, Italy) and transcardially perfused with phosphate-buffered saline (PBS) followed by 4% paraformaldehyde in PBS; their brains were removed, left in the fixative overnight, equilibrated in sucrose 30%, and cryopreserved at −80 °C. IHC was performed on serial sections cut transversely at 30–40 μm thickness at −25 °C in a cryomicrotome (Leica Camera; Leica Microsystems, Milan, Italy) from the brains embedded in Tissue-Tek OCT (Sakura, Milan, Italy). Sections were stained with an α-ChAT antibody (1:100; Santa Cruz, DBA, Milan, Italy) overnight. Primary antibody staining was revealed using Cy2-conjugated donkey anti-rabbit (Jackson Immuno Research, Milan, Italy). Nuclei were stained with Hoechst.

Quantification of cell number and volumes

For medial septum (MS)-diagonal band of Broca (DB), stereological analysis of the number of cells expressing ChAT was performed on one-in-four series of 30-μm free-floating coronal sections (120 μm apart), which were analyzed by confocal microscopy throughout the whole rostrocaudal extent of MS-DB (+1.18 to −0.34 from bregma). A total of nine sections were used for data analysis. The same sections and procedure were used to measure ChAT cells in caudate, as well as caudate volume. The reference space of the MS encompassed the triangular area that contains 95% or more of the basal forebrain cholinergic neurons dorsal to a line drawn across the tops of the anterior commissures. For hippocampus, stereological analysis of the number of cells was performed on one-in-six series of 40-μm free-floating coronal sections (240 μm apart) throughout the whole rostrocaudal extent of hippocampus (−0.94 to −3.08 from bregma). Total cell number was

obtained according to the optical dissector principle, by systematic sampling of counting frames of 100-μm sides in each section. ChAT-positive neurons that appeared in the different focal planes of the frame were included in the count, while ChAT-positive neurons in the uppermost focal plane of each section and intersecting the exclusion boundaries of the counting frame were excluded, as defined by the optical dissector principle. Total cell number (*N*) was calculated using the formula $N = Nv \times Vref$, where *N*v is the average cell number per dissector volume [corresponding to $100 \times 100 \times 30\ \mu m^3$ (for MS-DB, MS, and caudate) and $100 \times 100 \times 40\ \mu m^3$ (for hippocampus)] and *V*ref (reference volume) is the total volume of the MS, MS-DB, caudate, and hippocampus. The reference volume was obtained by multiplying the sum of the traced areas of MS, MS-DB, caudate, or hippocampus by distance between sections analyzed. Labeled cells and areas were measured by computer-assisted analysis using the IAS software (Delta Systems, Rome, Italy).

Western blotting

Equal amounts (10–30 μg) of proteins were separated on 4–12% Bis-Tris SDS-PAGE gels (Invitrogen, Milan, Italy), blotted onto PVDF membranes (Millipore, Prodotti Gianni, Milan, Italy), and incubated overnight with the appropriate primary antibody. The antibodies used were anti-β-actin (Sigma), α-ChAT, and α-TrkA (Santa Cruz).

Electrophysiology

Mice were anesthetized with isoflurane. Diaphragm preparations with the phrenic nerve supply intact were isolated and gently pinned flat in a sylgard-coated recording chamber. After the diaphragms had equilibrated for about an hour, the nerve was taken up into a suction electrode and the muscle fibers along the main intramuscular nerve branches were impaled with 3 M KCl-filled glass micropipettes (15–25 MΩ). Intracellular sharp-electrode recording was performed to record evoked EPPs in normal Ringer's solution (30 °C) containing 2.3-μM μ-conotoxin GIIIB (Bachem, CA, USA). The Ringer's solution was of the following composition (in mM): NaCl 116, KCl 4.5, $MgSO_4$ 1, $NaHCO_3$, 23, NaH_2PO_4 1, Dextrose 11, $CaCl_2$ 2. The stimulation pulses (0.01 ms) were applied via an AMPI Master-8 pulse generator and an AMPI Iso-Flex stimulus isolator. Potentials were amplified via a MultiClamp 700B amplifier (Axon Instruments, NY, USA), digitized at 10 kHz, and recorded to a computer using PCLAMP 9 software (Axon Instruments). Offline data analysis was performed using CLAMFIT 9 (Axon Instruments, NY, USA) and ORIGINPRO 7.5 (OriginLab, Northampton, MA, USA). In paired-pulse experiments, EPPs were elicited by nerve stimulation with supramaximal double pulses with interpulse interval range from 20 to 200 ms. Paired-pulse ration was evaluated by calculating the ratio of P2 to P1, where P2 is the EPP amplitude elicited by the second stimulus and P1 is the EPP amplitude elicited by the first stimulus.

Acknowledgments

This research was supported by Lunbeckfounden (R108-A10719 to CM) and European Molecular Biology Organization (ASTF264-2010 to C.M.); Alzheimer Association (IIRG-09-129984 and ZEN-11-201425 to L.D.); NIH (AG033007, AG041577 and AG041531 to L.D) and Thome Foundation (to L.D.); Italian Minister of Health (Project N 263/RF-2009-1536072 to M.A.-T.); the Regione Lazio, as part of the 'Distretto Tecnologico delle Bioscienze'; the research grant from FILAS Regione Lazio Funds for 'Sviluppo della Ricerca sul Cervello'. The funders had no role in study design, data collection and analysis, decision to publish, or preparation of the manuscript. We greatly appreciate the technical contribution of Maria Teresa Ciotti and the administrative support of Pamela Papa.

Author contributions

C.M. and L.D. designed the research; C.M., S.L., C.N., R.T., A.P., M.A.-T., L.R.L.R., Y.L., A.P.M.B., F.B., and F.L. performed the research; C.M., S.L, C.N., A.P., M.A.-T., L.R.L.R., H.Z, Y.L., R.T., and L.D. analyzed the data; C. M., S.L., and L.D. wrote the manuscript.

References

Ammassari-Teule M, Sgobio C, Biamonte F, Marrone C, Mercuri NB, Keller F (2009) Reelin haploinsufficiency reduces the density of PV+ neurons in circumscribed regions of the striatum and selectively alters striatal-based behaviors. *Psychopharmacology* **204**, 511–521.

Arendt T (2009) Synaptic degeneration in Alzheimer's disease. *Acta Neuropathol.* **118**, 167–179.

Barbagallo AP, Weldon R, Tamayev R, Zhou D, Giliberto L, Foreman O, D'Adamio L (2010) Tyr682 in the intracellular domain of APP regulates amyloidogenic APP processing in vivo. *PLoS ONE* **5**, e15503.

Barbagallo AP, Wang Z, Zheng H, D'Adamio L (2011) A single tyrosine residue in the amyloid precursor protein intracellular domain is essential for developmental function. *J. Biol. Chem.* **286**, 8717–8721.

Bovet D, Bovet-Nitti F, Oliverio A (1969) Genetic aspects of learning and memory in mice. *Science* **163**, 139–149.

Calissano P, Matrone C, Amadoro G (2010) NGF as a paradigm of neurotrophins related to Alzheimer's disease. *Dev. Neurobiol.* **70**, 372–383.

D'Amato FR, Zanettini C, Sgobio C, Sarli C, Carone V, Moles A, Ammassari-Teule M (2011) Intensification of maternal care by double-mothering boosts cognitive function and hippocampal morphology in the adult offspring. *Hippocampus* **21**, 298–308.

Dawson GR, Seabrook GR, Zheng H, Smith DW, Graham S, O'Dowd G, Bowery BJ, Boyce S, Trumbauer ME, Chen HY, Van Der Ploeg LHT, Sirinathsinghji DJS (1999) Age-related cognitive deficits, impaired long-term potentiation and reduction in synaptic marker density in mice lacking the β-amyloid precursor protein. *Neuroscience* **90**, 1–13.

Fotinopoulou A, Tsachaki M, Vlavaki M, Poulopoulos A, Rostagno A, Frangione B, Ghiso J, Efthimiopoulos S (2005) BRI2 interacts with amyloid precursor protein (APP) and regulates amyloid beta (Abeta) production. *J. Biol. Chem.* **280**, 30768–30772.

Hardy J, Selkoe DJ (2002) The amyloid hypothesis of Alzheimer's disease: progress and problems on the road to therapeutics. *Science* **297**, 353–356.

Li H, Wang Z, Wang B, Guo Q, Dolios G, Tabuchi K, Hammer RE, Südhof TC, Wang R, Zheng H (2010) Genetic dissection of the amyloid precursor protein in developmental function and amyloid pathogenesis. *J. Biol. Chem.* **285**, 30598–30605.

Luvisetto S, Marinelli S, Rossetto O, Montecucco C, Pavone F (2004) Central injection of botulinum neurotoxins: behavioural effects in mice. *Behav. Pharmacol.* **15**, 233–240.

Luvisetto S, Basso E, Petronilli V, Bernardi P, Forte M (2008) Enhancement of anxiety, facilitation of avoidance behaviour, and occurrence of adult-onset obesity in mice lacking mitochondrial cyclophilin D. *Neuroscience* **155**, 585–596.

Massett MP, Berk BC (2005) Strain-dependent differences in responses to exercise training in inbred and hybrid mice. *Am. J. Physiol. Regul. Integr. Comp. Physiol.* **288**, R1006–R1013.

Matrone C, Ciotti MT, Marolda R, Mercanti D, Calissano P (2008) NGF and BDNF control amyloidogenic route and Ab production in hippocampal neurons. *Proc. Natl. Acad. Sci. USA* **105**, 13139–13144.

Matrone C, Marolda R, Ciotti MT, Ciafrè S, Mercanti D, Calissano P (2009) Tyrosine Kinase NGF receptor switches from pro-survival to pro-apoptotic activity via Abeta mediated phosphorylation. *Proc. Natl. Acad. Sci. USA* **106**, 11358–11360.

Matrone C, Barbagallo AP, La Rosa LR, Florenzano F, Ciotti MT, Mercanti D, Chao MV, Calissano P, D'Adamio L (2011) APP is phosphorylated by TrkA and regulates NGF/TrkA signaling. *J. Neurosci.* **31**, 11756–11761.

Matsuda S, Matsuda Y, D'Adamio L (2003) Amyloid beta protein precursor (AbetaPP), but not AbetaPP-like protein 2, is bridged to the kinesin light chain by the scaffold protein JNK-interacting protein 1. *J. Biol. Chem.* **278**, 38601–38606.

Matsuda S, Giliberto L, Matsuda Y, Davies P, McGowan E, Pickford F, Ghiso J, Frangione B, D'Adamio L (2005) The familial dementia BRI2 gene binds the Alzheimer gene amyloid-beta precursor protein and inhibits amyloid-beta production. *J. Biol. Chem.* **280**, 28912–28916.

Matsuda S, Giliberto L, Matsuda Y, McGowan EM, D'Adamio L (2008) BRI2 inhibits amyloid beta-peptide precursor protein processing by interfering with the docking of secretases to the substrate. *J. Neurosci.* **28**, 8668–8676.

Matsuda S, Matsuda Y, Snapp EL, D'Adamio L (2011) Maturation of BRI2 generates a specific inhibitor that reduces APP processing at the plasma membrane and in endocytic vesicles. *Neurobiol. Aging* **32**, 1400–1408.

Niewiadomska G, Mietelska-Porowska A, Mazurkiewicz M (2011) The cholinergic system, nerve growth factor and the cytoskeleton. *Behav. Brain Res.* **221**, 515–526.

Roncarati R, Sestan N, Scheinfeld MH, Berechid BE, Lopez PA, Meucci O, McGlade JC, Rakic P, D'Adamio L (2002) The gamma-secretase-generated intracellular domain of beta-amyloid precursor protein binds numb and inhibits notch signaling. *Proc. Natl. Acad. Sci. USA* **99**, 7102–7107.

Ruberti F, Capsoni S, Comparini A, Di Daniel E, Franzot J, Gonfloni S, Rossi G, Berardi N, Cattaneo A (2000) Phenotypic knockout of nerve growth factor in adult transgenic mice reveals severe deficits in basal forebrain cholinergic neurons, cell death in the spleen, and skeletal muscle dystrophy. *J. Neurosci.* **20**, 2589–2601.

Russo C, Dolcini V, Salis S, Venezia V, Zambrano N, Russo T, Schettini G (2002) Signal transduction through tyrosine-phosphorylated C-terminal fragments of amyloid precursor protein via an enhanced interaction with Shc/Grb2 adaptor proteins in reactive astrocytes of Alzheimer's disease brain. *J. Biol. Chem.* **277**, 35282–35288.

Scheinfeld MH, Matsuda S, D'Adamio L (2003a) JNK-interacting protein-1 promotes transcription of A beta protein precursor but not A beta precursor-like proteins, mechanistically different than Fe65. *Proc. Natl. Acad. Sci. USA* **100**, 1729–1734.

Scheinfeld MH, Ghersi E, Davies P, D'Adamio L (2003b) Amyloid beta protein precursor is phosphorylated by JNK-1 independent of, yet facilitated by, JNK-interacting protein (JIP)-1. *J. Biol. Chem.* **278**, 42058–42063.

Schliebs R, Arendt T (2011) The cholinergic system in aging and neuronal degeneration. *Behav. Brain Res.* **221**, 555–563.

Taglialatela G, Hogan D, Zhang WR, Dineley KT (2009) Intermediate- and long-term recognition memory deficits in Tg2576 mice are reversed with acute calcineurin inhibition. *Behav. Brain Res.* **200**, 95–99.

Tamayev R, Zhou D, D'Adamio L (2009) The interactome of the amyloid beta precursor protein family members is shaped by phosphorylation of their intracellular domains. *Mol. Neurodegener.* **4**, 28.

Tamayev R, Matsuda S, Giliberto L, Arancio O, D'Adamio L (2011) APP heterozygosity averts memory deficit in knockin mice expressing the Danish dementia BRI2 mutant. *EMBO J.* **30**, 2501–2509.

Tamayev R, Matsuda S, Arancio O, D'Adamio L (2012) beta- but not gamma-secretase proteolysis of APP causes synaptic and memory deficits in a mouse model of dementia. *EMBO Mol. Med.* **4**, 171–179.

Tarr PE, Roncarati R, Pelicci G, Pelicci PG, D'Adamio L (2002) Tyrosine phosphorylation of the beta-amyloid precursor protein cytoplasmic tail promotes interaction with Shc. *J. Biol. Chem.* **277**, 16798–16804.

Vidal R, Frangione B, Rostagno A, Mead S, Revesz T, Plant G, Ghiso J (1999) A stop-codon mutation in the BRI gene associated with familial British dementia. *Nature* **399**, 776–781.

Yang L, Wang B, Long C, Wu G, Zheng H (2007) Increased asynchronous release and aberrant calcium channel activation in amyloid precursor protein deficient neuromuscular synapses. *Neuroscience* **149**, 768–778.

Zhou D, Noviello C, D'Ambrosio C, Scaloni A, D'Adamio L (2004) Growth factor receptor-bound protein 2 interaction with the tyrosine-phosphorylated tail of amyloid beta precursor protein is mediated by its Src homology 2 domain. *J. Biol. Chem.* **279**, 25374–25380.

Zhou D, Zambrano N, Russo T, D'Adamio L (2009) Phosphorylation of a tyrosine in the amyloid-beta protein precursor intracellular domain inhibits Fe65 binding and signaling. *J. Alzheimers Dis.* **16**, 301–307.